Nano Energy 34 (2017) 515–523

Contents lists available at ScienceDirect

Nano Energy

journal homepage: www.elsevier.com/locate/nanoen

Communication

Direct anodic exfoliation of graphite onto high-density aligned graphene for large capacity supercapacitors

Liangsheng Hu[a,1], Xiang Peng[b,1], Yong Li[a], Lei Wang[c], Kaifu Huo[c,*], Lawrence Yoon Suk Lee[a], K.Y. Wong[a,*], Paul K. Chu[b,*]

[a] Department of Applied Biology and Chemical Technology and the State Key Laboratory of Chirosciences, The Hong Kong Polytechnic University, Hung Hom, Kowloon, Hong Kong, China
[b] Department of Physics and Materials Science, City University of Hong Kong, Tat Chee Avenue, Kowloon, Hong Kong, China
[c] Wuhan National Laboratory for Optoelectronics (WNLO) and School of Optical and Electronic Information, Huazhong University of Science and Technology, Wuhan 430074, China

ARTICLE INFO

Keywords:
Aligned graphene
Supercapacitor
Electrochemical exfoliation
Energy storage

ABSTRACT

Vertically oriented graphene nanosheets (VOGNs) fabricated on conductive substrates with a large amount of edge planes and open channels are ideal for electrochemical double-layer (EDL) capacitor electrodes. However, preparation of such a structure with high-density of graphene nanosheets is challenging. Herein, a facile, environment-friendly, and economical technique to prepare high-quality VOGNs directly on conductive graphite plates with a high mass loading is described. The VOGNs are obtained by electrochemical anodization of graphite and a large amount of aligned reduced graphene oxide (rGO) is produced and adheres strongly to the graphite substrate (G@rGO). The symmetrical supercapacitors composed of the G@rGO electrodes exhibit a high volumetric capacitance of 3.9 F cm^{-3} and energy density of 0.66 Wh L^{-1} (based on the volume of the whole electrode) at a current density of 7.5 mA cm^{-3} in 6 M KOH. The rate performance and long-term cycling stability are very good. The outstanding capacitive performance can be attributed to the unique structure of the G@rGO electrode which facilitates transportation of ions between the electrolyte and graphene surface, minimizes the distributive nature of charge storage, expedites the formation of EDL, and enhances the electrochemical utilization of graphene and stability by avoiding restacking and aggregation of graphene nanosheets.

1. Introduction

Supercapacitors, also known as electrochemical double-layer (EDL) capacitors or ultracapacitors, have attracted a great deal of attention due to their high power density, long cycle life, simple principles, fast dynamics of charge propagation, and low maintenance cost [1–8]. Fundamentally, supercapacitors operate by storing ions within the EDL or through redox reactions on the electrode surface [9]. Carbon-based materials such as activated carbon [10,11], activated carbon cloths [12,13], porous carbon spheres [14,15], carbon onions [16,17], carbon nanotubes [18,19], mesoporous carbons [20–22], and graphene [23–28] have been investigated as electrode materials in supercapacitors on account of the unique combination of the large specific surface area (SSA), light weight, as well as good electrical conductivity. Among the various nanostructured carbon materials [29,30], graphene, a two-dimensional (2D) hexagonal lattice of sp^2 hybridized carbon atoms containing a large network of delocalized π-electrons [31], is promising because of its high electrical conductivity and large theoretical specific surface area (~2630 m^2 g^{-1}) [32]. In principle, graphene sheets (single layer or few layers) which can have a capacitance as high as 550 F g^{-1} [2,32] have immense potential as next-generation electrode materials in energy storage. However, the practical performance of graphene-based supercapacitors falls short of the ideal one due to various reasons. Firstly, the strong Van der Waals interactions between adjacent sheets inevitably cause restacking and aggregation in the graphene assemblies consequently reducing the inter-sheet open channels and actual electrochemically accessible electrode surface area [30,33,34]. Secondly, most graphene-based materials are oriented randomly or parallel to the current collectors in the supercapacitor and hence, it is not easy for electrolyte ions to permeate deeply inside the graphene layers [35,36] resulting in incomplete utilization of the electrochemical surface area of graphene and limiting the extent of

* Corresponding authors.
E-mail addresses: kfhuo@hust.edu.cn (K. Huo), kwok-yin.wong@polyu.edu.hk (K.Y. Wong), paul.chu@cityu.edu.hk (P.K. Chu).
[1] These authors contributed equally to this work.

http://dx.doi.org/10.1016/j.nanoen.2017.03.007
Received 20 January 2017; Received in revised form 3 March 2017; Accepted 3 March 2017
Available online 12 March 2017

EDL. Thirdly, the large contact resistance between graphene and current collectors compromises the performance [37–39].

Recently, vertically oriented graphene nanosheets (VOGNs), a unique morphology of few-layered graphene sheets aligned in an open and interconnected, three-dimensional (3D) array, have demonstrated notable charge storage features including the high-rate capability, specific capacitance, and stability because their favorable structural and electrochemical properties overcome the aforementioned problems that plague conventional graphene-based EDL capacitor electrodes [1,36,40–45]. In VOGNs, abundant edge planes are exposed thus providing larger capacitance than the basal planes. The non-agglomerated morphology together with a large surface-to-volume ratio and open channels between the sheets offers high conductance channels for ingress and egress of electrolyte ions to reduce the ionic resistance. The open structure and exposure of active sites from edge planes not only facilitate transportation of ions between the electrolyte and graphene surfaces to minimize the distributive nature of charge storage and expedite the formation of EDL, but also enhance electrochemical utilization of graphene and stability by avoiding restacking and aggregation of the graphene nanosheets. In addition, if the VOGNs are prepared directly on a conductive surface (current collector) without a binder, lower contact resistance between the active materials and current collectors and high power capability of the EDL capacitors are expected. However, most of the reported VOGNs have been produced by chemical vapor deposition or plasma-enhanced chemical vapor deposition, in which only a small quantity of graphene can be loaded onto the current collectors and the small mass loading of active VOGNs leads to low areal and volumetric capacitance. Prolonging the preparation time in these methods may not produce a thicker VOGNs structure, but instead often results in the formation of undesired amorphous carbon [36]. Therefore, it is important to develop a simple, mild, low-cost, and green method to produce high-quality VOGNs with a large mass loading.

Graphene is usually prepared by mechanical [46] or chemical [47] exfoliation, chemical vapor deposition [48], solvent- and surfactant-assisted liquid-phase exfoliation [49], electrochemical expansion [50],

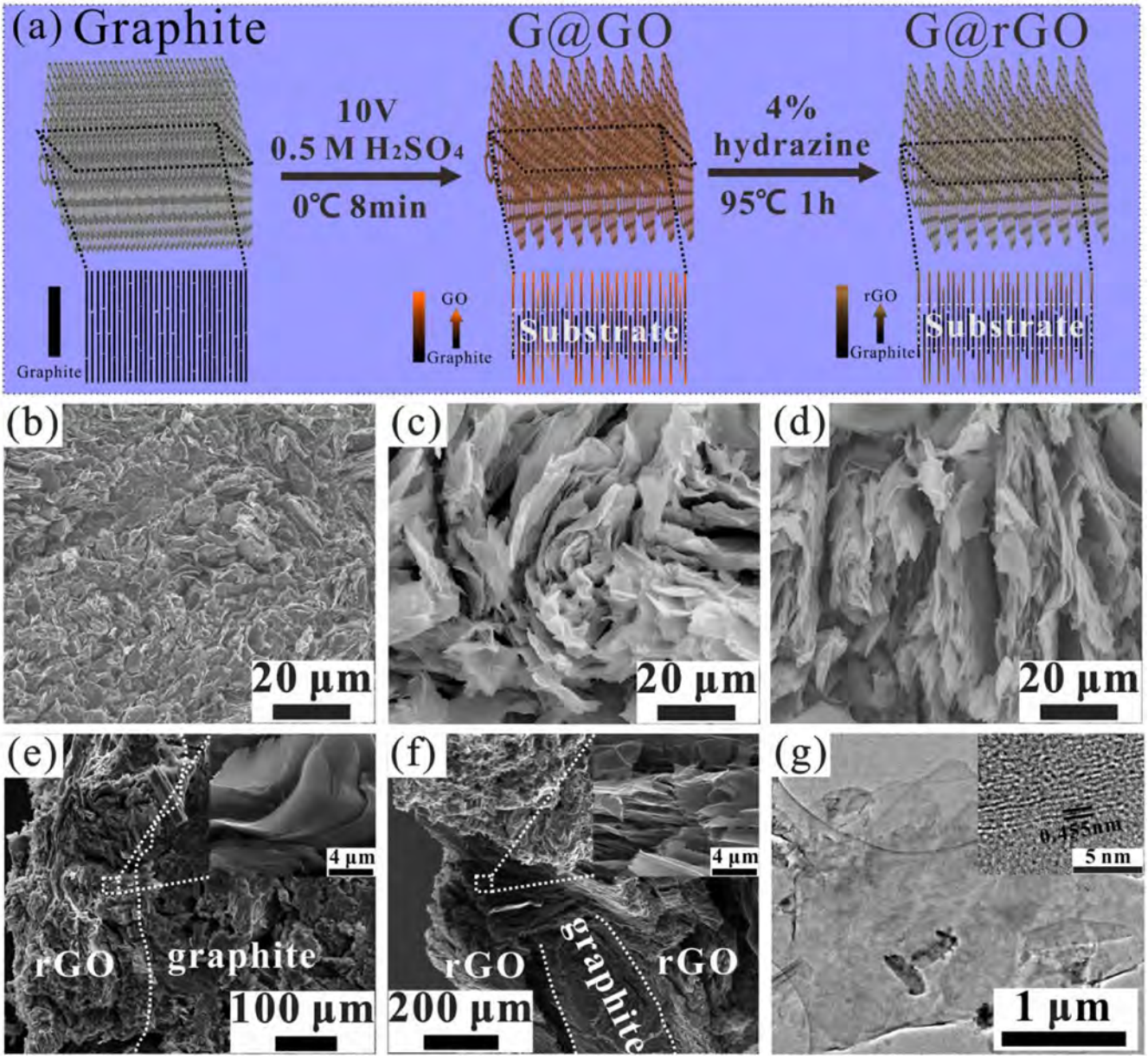

Fig. 1. (a) Schematic diagram showing the fabrication process of G@rGO; Top-view FE-SEM images of (b) natural graphite, (c) G@GO, and (d) G@rGO; (e) Cross-sectional and (f) longitudinal-view images of G@rGO; (g) TEM image of typical rGO layers. The inset in (g) is an HR-TEM image of the corresponding rGO layers.

and electrochemical exfoliation [51–58]. Among them, electrochemical exfoliation is one of the preferred techniques because of the simplicity, low cost, efficiency, and environmental friendliness. So far, almost all research activities have focused on graphene exfoliation from graphite, but little attention has been paid to the products remaining on the surface of the exfoliated graphite. In this work, we demonstrate a simple, environmentally friendly, efficient, and economical method to prepare high-quality VOGNs on graphite plates with a large mass loading for high-performance graphene-based supercapacitor electrodes. After electrochemical anodization and hydrazine reduction, a large amount of aligned reduced graphene oxide (rGO) with strong adhesion to the graphite substrate is produced (G@rGO) as schematically shown in Fig. 1**a**. This method is suitable for graphite with different shape and applicable to electrodes requiring a special shape. The G@rGO electrodes with the unique structure deliver outstanding capacitive performance and are suitable for high-performance supercapacitors.

2. Experimental section

2.1. G@GO and G@rGO fabrication

The natural graphite flakes (1×1.2×0.08 cm^3, Beijing Dingsheng Kaixiang Trading Co., Ltd.) were adhered to a copper wire with silver paint and insulated with epoxy resin to expose both sides (area of 1×1 cm^2) to serve as the anode in electrochemical exfoliation. A Pt foil (2×2 cm^2) was used as the cathode electrode. The graphite and Pt foils were placed in parallel on a shelf at a distance of 5 cm and immersed in a H_2SO_4 (0.5 M) solution in an ice bath. Electrochemical anodization was carried out by applying a positive DC voltage (+10 V) to the graphite electrode for different time durations with regular intervals (every 30 s). A sufficient suspension time was necessary to cool the H_2SO_4 (0.5 M) solution to 0 °C before starting the next period with regard to efficient fabrication of high-density graphene arrays. The specific voltage (10 V) chosen on the basis of recent studies of anodic exfoliation of graphite in an aqueous electrolyte applied to the graphite anode in H_2SO_4 led to expansion and detachment of small fragments of the materials [51–58]. For comparison, two control experiments were carried out: (1) Electrochemical anodization performed continuously for 8 min at room temperature (25 °C) and (2) artificial graphite plates used instead of natural graphite flakes. After electrochemical exfoliation, the graphite was sonicated in deionized water for 30 s to remove loose graphene oxide fragments and the vertically oriented graphene oxide nanosheets were fabricated on the graphite surface (designated as G@GO). In the typical procedure for chemical conversion of G@GO to G@rGO, G@GO was immersed in 50 mL of 4% hydrazine solution in a 100 mL glass flask and the glass flask was put in a water bath (~95 °C) for 1 h.

2.2. G@GO and G@rGO characterization

The products and graphite plates were characterized by field-emission scanning electron microscopy (FE-SEM, FEI Nova 400 Nano), transmission electron microscopy (TEM), high-resolution TEM (HR-TEM, JEOL, JEM-2100F), Raman scattering (Renishaw 2000), and X-ray photoelectron spectroscopy (XPS, Physical Electronics PHI 5802).

2.3. Electrochemical measurement

The electrochemical experiments were conducted based on a three-electrode system on the CHI 6144D electrochemical workstation (CH Instruments, Shanghai, China) in 6 M KOH with a Pt foil (1×1 cm^2) as a counter electrode, saturated calomel electrode (SCE) as the reference electrode, and G@rGO as the working electrode. Two pieces of the G@rGO electrodes were assembled in the supercapacitor together with a separator (NKK TF40, Japan). The properties were determined by cyclic voltammetry (CV) and galvanostatic charging/discharging (GC). Electrochemical impedance spectroscopy (EIS) was performed from 10 mHz to 100 kHz with a potential amplitude of 5 mV and the cycling life was assessed by GC at a current density of 75 mA cm^{-3}.

3. Results and discussion

3.1. Characterization of G@GO and G@rGO

Fig. 1**a** illustrates the electrochemical fabrication process of G@rGO and the corresponding morphologies are shown in Figs. 1**b-f**. The G@rGO-8 is obtained by electrochemically anodizing graphite at 10 V in 0 °C H_2SO_4 (0.5 M) for 8 min and subsequent reduction in a 4% hydrazine solution at ~95 °C for 1 h (See Experimental Section for details). Figs. 1**b-f** depict the FE-SEM images of the starting material/graphite (Fig. 1**b**), prepared graphene oxide (GO) on the graphite substrate (G@GO) (Fig. 1**c**), and G@rGO (Figs. 1**d–f**), respectively. The FE-SEM image of the untreated graphite shows a continuous surface composed of many quasi-vertical edge planes and a few basal planes (Fig. 1**b**). After the electrochemical treatment, a dense, porous, and vertically aligned 3-D network of thin GO nanosheets array is produced (Fig. 1**c**). Subsequent reduction of G@GO to G@rGO with hydrazine does not change the topography of the sample (Fig. 1**d**). The cross-sectional view of the G@rGO shows an elastic boundary between the rGO layer and graphite as well as a regularly arranged rGO layer (Inset in Fig. 1**e**) with a thickness of ~220 μm nearly vertical to the graphite (Fig. 1**e**). The longitudinal-view FE-SEM image of G@rGO reveals a core–sheath structure consisting of a graphite core with a thickness of ~210 μm and a ~220 μm thick and well-defined rGO sheath (Inset in Fig. 1**f**), confirming the production of 3-D VOGNs on

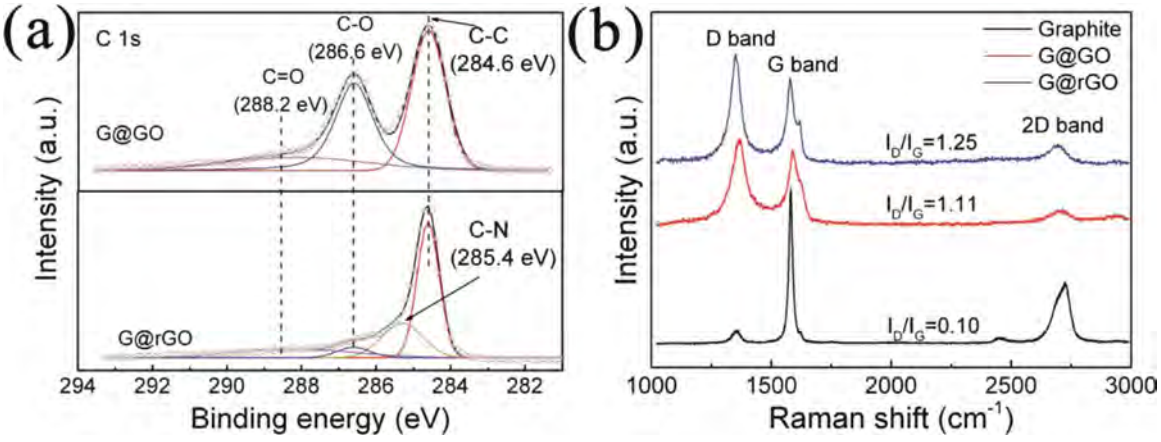

Fig. 2. (a) High-resolution C 1s XPS spectra of G@GO and G@rGO and (b) Raman spectra of graphite, G@GO, and G@rGO.

graphite (Fig. 1**f**). The produced rGO sheath is estimated to have a mass loading of about 18 mg cm^{-2} (both sides) and the mass fraction of the rGO is approximately 31% of the G@rGO. The TEM and HR-TEM images of the rGO in Fig. 1**g** clearly disclose that the rGO network consists of few-layer (3–6 layers) graphene sheets. The interlayer spacing is 0.455 nm that is larger than the d-spacing of graphite (0.335 nm), showing that the initially stacked graphite layers are converted into well-exfoliated graphene sheets by the anodic treatment. Similar phenomena have been observed [56,59] and the larger d-spacing is believed to facilitate ions movement between graphitic layers [60].

XPS is performed to determine the chemical composition and states of G@GO and G@rGO. The survey spectrum of G@rGO (Fig. S1 in Supporting Information) shows a strong peak at 400.1 eV associated with N in addition to peaks arising from C and O similar to those observed from G@GO. This indicates that the hydrazine reduction procedures not only reduce the GO to rGO, but also introduce nitrogen (3 at%) to graphene [61,62]. The high-resolution XPS C 1 s spectra of G@GO and G@rGO are displayed in Fig. 2**a**. G@GO shows two main peaks at 284.6 and 286.6 eV corresponding to sp^2 carbon and C–O bond, respectively, and the broad shoulder at 288.2 eV is related to C=O [63]. With regard to G@rGO, the peaks corresponding to C–O and C=O appear from the same region, but their intensity is reduced as the C/O ratio is increased from 2.48 (G@GO) to 6.89. Additionally, there is an obvious peak at 285.4 eV for C–N further verifying that N is incorporated into the reduced graphene [61,62]. Raman scattering spectra acquired from pristine graphite, G@GO, and G@rGO are shown in Fig. 2**b**. The two prominent G and 2D bands as well as a small D band of pristine graphite are located at 1580, 2720, and 1353 cm^{-1}, respectively, showing a D/G ratio (I_D/I_G) of 0.10 (Fig. 2**b** black line) matching the normal characteristics of typical graphitic structures [64]. After the electrochemical treatment, the positions of the D, G, and 2D bands shift to 1368, 1593 and 2702 cm^{-1}, respectively (Fig. 2**b** red line), suggesting destruction of the graphitic structure and size reduction of the in-plane sp^2 domains [65]. The Raman spectrum of rGO (Fig. 2**b** blue line) also exhibits the G and D bands at 1580 and 1351 cm^{-1}, respectively, together with a larger I_D/I_G (1.25) than that of GO (1.11), indicating further decrease in the average size of the sp^2 domains upon reduction of GO. The D′ band that appears as a shoulder at 1620 cm^{-1} in the spectra of both GO and rGO is generally associated with disorders or defects in carbon materials [66]. Compared to graphite, the intensity of the 2D band of both GO and rGO is smaller mainly attributable to disorder along the c-axis [64].

Control of the structure and morphology is key to the fabrication of carbon-based electrodes in order to allow effective permeation of the electrolyte to establish EDLs in the supercapacitors. In order to systematically explore the morphological changes during the electrochemical treatment process and optimize the EDL capacitance of the resulting VOGNs, a DC voltage of +10 V is applied to the graphite electrodes for different time durations (1, 3, 5, 8, and 10 min, designated as G@rGO-1, −3, −5, −8, and −10, respectively) followed by the same hydrazine reduction treatment. Figs. 3**a-e** and **S2** depict the top and longitudinal FE-SEM images of G@rGO, respectively. Compared to the continuous surface of the raw graphite, few cracks appear from the surface of G@rGO (Fig. 3**a**). When the processing time is increased to 3 min, more cracks emerge and many graphite layers are split from each other (Fig. 3**b**). By prolonging the time to 5 min, some large voids with a size of up to micrometers appear between the cleaved layers (Fig. 3**c**). The image of the 8 min sample (Fig. 3**d**) shows that most of the graphite layers are split and VOGNs are formed. If the time is extended to more than 10 min, it is difficult to observe a regular graphene network on graphite (Fig. 3**e**). The corresponding longitudinal view (Fig. S2) shows that the thickness of the aligned rGO layer increases gradually from 10 to 220 μm as the anodic time is increased from 1 to 8 min. However, no further increase is visible if the time is more than 8 min (Fig. 2**f**). Raman scattering (Fig. S3) is employed to monitor the changes in the surface states with time and as the time is increased, I_D/I_G increases gradually indicating a more disordered structure.

According to the literature [51–58], the possible formation process

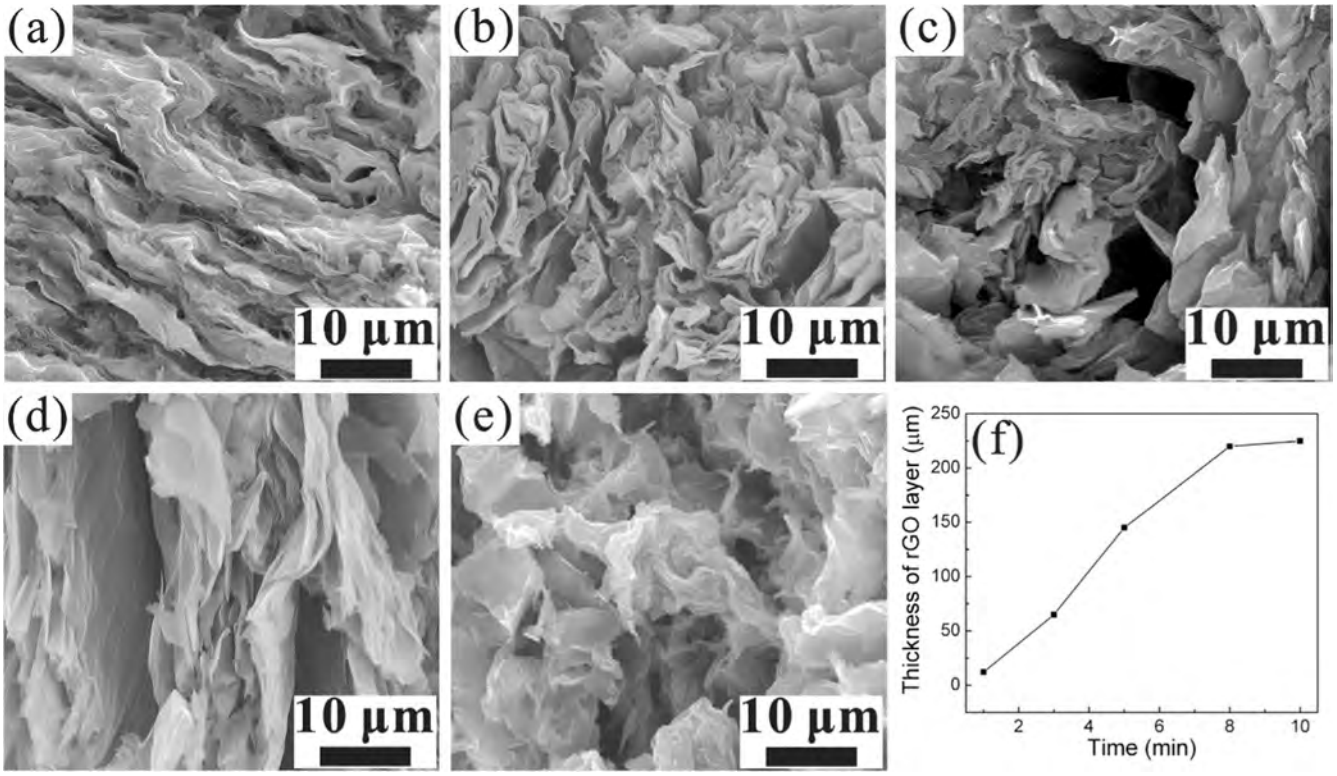

Fig. 3. FE-SEM images showing the top-view morphology of G@rGO for different exfoliation time: (a) 1 min, (b) 3 min, (c) 5 min, (d) 8 min, and (e) 10 min; (f) Corresponding thickness of the rGO layer.

of VOGNs is described in the following. When a positive voltage (+10 V) is applied to graphite, the bias voltage gives rise to oxidation and generation of hydroxyl (OH•) and oxygen (O•) radicals. Intercalation of SO_4^{2-} into defect sites and grain boundaries of graphite induce splitting due to oxidation or hydroxylation by OH• and O• radicals. Meanwhile, oxidation or hydroxylation generates gaseous species such as SO_2 and O_2 causing the small graphite layers to detach from the substrate/graphite and separation of weakly bound graphite layers from one another. If the graphite is electrochemically treated for a moderate period of time (*e.g.*, 8 min), the small graphite layers are removed from the graphite substrate while the large cleaved graphite layers remain on the surface of graphite forming VOGNs.

The effects of the electrolyte temperature on graphite exfoliation and formation of VOGNs are investigated. Fig. S4 shows the top-sectional and longitudinal FE-SEM images of G@rGO that is electrochemically prepared at room temperature (25 °C) continuously for 8 min. Many macropores or voids and only a thin fringe of graphene nanosheets are produced on the surface of graphite (Fig. S4a). The longitudinal FE-SEM image shows that the thickness of the graphene layer is about 80 μm (Fig. S4b) which is substantially smaller than that of (~220 μm) G@rGO prepared in an ice bath with regular intervals of suspension. The results suggest that it is essential to suspend the anodic treatment with regular intervals as well as low temperature to ensure fabrication of uniform and thick graphene layers on graphite, otherwise the heated solution enhances exfoliation resulting in the production of a large quantity of gas (SO_2 and O_2) at the defect sites or boundaries of the graphite. This consequently leads to rapid detachment of the cleaved graphene sheets from the substrate and less split graphene sheets remain. In addition, a control experiment is performed to study the effect of the degree of graphitization on the structure and morphology of the products. Low degree of graphitization of the artificial graphite plate with an I_D/I_G ratio of 0.68 (Fig. S5) is used as the starting graphite in electrochemical exfoliation. The top-sectional FE-SEM image in Fig. S6 reveals that only patches of the scattered thick-sheets remain on the surface of graphite and the longitudinal FE-SEM image shows that the thickness of the sheet layer is only 20 μm, indicating that a high degree of graphitization of the starting graphite is also necessary for successful synthesis of VOGNs.

3.2. Performance of G@rGO as supercapacitor electrodes

The electrochemical performance of the G@rGO electrodes is evaluated on the three-electrode system in a 6 M KOH aqueous electrolyte. For comparison and optimization of the electrochemical treatment of the graphite, the effects of different exfoliation temperature are investigated. The results in Fig. S7 show that anodic exfoliation conducted at 0 °C with regular intervals of suspension leads to higher capacitance than at room temperature. The pristine graphite has a large effect on the capacitive performance of the G@rGO electrode. As shown in Fig. S8, the G@rGO electrode fabricated from artificial graphite with a larger I_D/I_G ratio of 0.68 (Fig. S5) has a smaller capacitance than that prepared from natural graphite with the I_D/I_G ratio of 0.10. The relatively poorer capacitive performance may be ascribed to the smaller amount of rGO on graphite as shown in Figs. S4 and S6. Therefore, in this work, natural graphite is used as the starting graphite materials and the exfoliation experiments are conducted at 0 °C in an ice bath with regular intervals of suspension. Fig. 4**a** shows the CV profiles of the graphite electrode (0 min) and G@rGO electrodes exfoliated for different times at a scanning rate of 100 mV s^{-1}. For the graphite electrode, no obvious EDL performance is observed, while the near rectangular curves observed from the G@rGO electrodes indicate the typical EDL capacitive behavior. With increasing exfoliation time, the current density in the CV curves obtained from the G@rGO electrodes increases gradually and the maximum areal capacitance is observed from G@rGO-8. However, the G@rGO electrode performs decreased specific capacitance if the time is increased further, *e.g.*, 10 min, presumably because more generated graphene is detached from the graphite substrate (Fig. 2). A similar trend is observed from the corresponding GC plots **(**Fig. 4**b)** at a current density of 1 mA cm^{-2}. Meanwhile, the GC curves show a nearly symmetrical triangular shape without an obvious voltage drop, suggesting good charge transfer in the G@rGO electrodes as well as highly reversible and ideal EDL capacitor behavior.

Fig. 4**c** presents the cyclic voltammograms of the G@rGO-8 electrode acquired at different scanning rates between 10 and 200 mV s^{-1}. The integrated area in the voltammogram increases as the scanning rate is increased without losing the rectangular shape even at 200 mV s^{-1}, reflecting the characteristics of an EDL capacitor with high reversibility and excellent rate capability. GC curves are

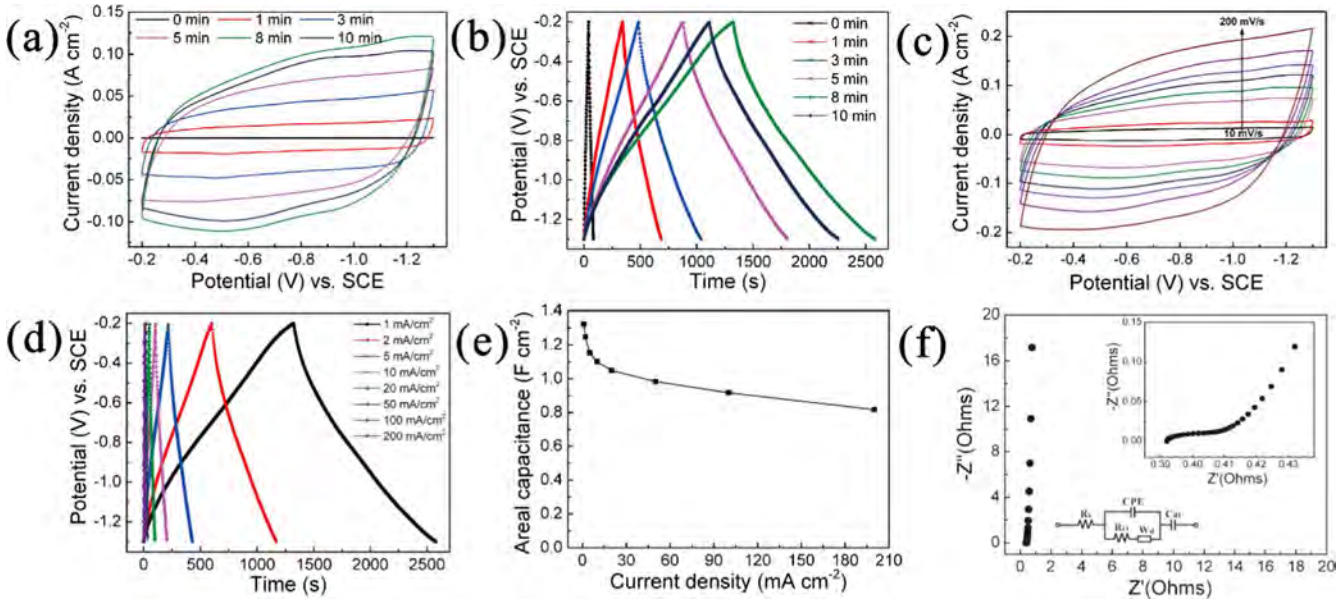

Fig. 4. Electrochemical performance of the electrode: (a) CV and (b) GC curves of graphite oxidized for different times at a scanning rate of 100 mV s^{-1} and current density of 1 mA cm^{-2}; (c) CV profiles of G@rGO-8 at scanning rates between 10 and 200 mV s^{-1}; (d) GC plots of G@rGO-8 at current densities between 1 and 200 mA cm^{-2}; (e) Areal capacitance as a function of current densities of the G@rGO-8 electrode; (f) Nyquist plot of G@rGO-8.

acquired at different current densities to study the specific capacitance and rate capability of the G@rGO-8 electrode, as shown in Fig. 4**d**. The specific capacitance can be calculated by the following formula: $C_s=I\Delta t/A\Delta E$, where C_s (mF cm^{-2}) is the areal specific capacitance based on the geometric area of the G@rGO-8 electrode, I (mA) is the discharge current, Δt (s) is the discharging time after full charging, A (cm^2) is the geometric area of the electrode, and ΔE (V) is the voltage window during discharging. The calculated areal capacitance as a function of current density is displayed in Fig. 4**e** which indicates that the capacitance of the G@rGO-8 electrode is as large as 1.3 F cm^{-2} at a current density of 1 mA cm^{-2}. The rGO mainly contributes to the capacitance of the G@rGO-8 electrode as graphite has negligible specific capacitance (0.03 F cm^{-2}, Fig. 4**b**). Even at a large current density of 200 mA cm^{-2}, the capacitance reaches 0.8 F cm^{-2}, implying that more than 60% of the specific capacitance is retained even when the current density is increased by 200 folds. The capacitance of the G@rGO-8 electrode here is larger than those of recently reported carbon-based materials and even some pseudocapacitive metal oxides and composite electrodes such as electrochemically activated carbon cloth (EACC, 756 mF cm^{-2} at 6 mA cm^{-2}) [13], Ni/Co_3O_4 (410 mF cm^{-2} at 5.6 mA cm^{-2}) [67], $NiCo_2O_4$ electrode (858.3 mF cm^{-2} at 6.7 mA cm^{-2}) [68], WO_{3-x}/MoO_{3-x} (303 mF cm^{-2} at 5 mA cm^{-2}) [69], PANI/TiN/PANI coaxial nanotube arrays (193 mF cm^{-2} at 1 mA cm^{-2}) [70], and MoOx/TiN nanotube arrays (165 mF cm^{-2} at 1 mA cm^{-2}) [71]. Our results demonstrate that the G@rGO-8 electrode has high specific capacitance and excellent rate capability. The outstanding capacitive performance can be attributed to the ideal structure of the vertical rGO nanosheets firmly bonded to the highly conductive graphite substrate/current collector with a large exposed active area, smooth electrolyte channel, as well as low inner resistance and charge transfer resistance as confirmed by EIS in Fig. 4**f**. The Nyquist plot obtained from the G@rGO-8 electrode in Fig. 4**f** is nearly vertical to the axis of the real component of the impedance and the phase angle is near −90° at low frequencies (see Fig. S9), further verifying the ideal EDL capacitive behavior of the G@rGO-8 electrode [1,2,40,72]. The G@rGO-8 electrode shows a small charge transfer resistance of less than 0.02 Ω consistent with the large specific capacitance and excellent rate capability of the G@rGO-8 electrode.

To evaluate the performance of the G@rGO in supercapacitors, the symmetrical supercapacitor is assembled with two G@rGO electrodes (Fig. 5**)**. Fig. 5**a** presents the CV curves of the G@rGO-based supercapacitor at scanning rates between 10 and 200 mV s^{-1} and excellent reversibility even at a large scanning rate of 200 mV s^{-1} is observed. The GC curves in Fig. 5**b** illustrate that the volumetric capacitance can reach 3.9 F cm^{-3} at a current density of 7.5 mA cm^{-3} based on the entire volume of the two electrodes including the graphite substrate. Even at a large current density of 150 mA cm^{-3}, the volumetric capacitance is 3.1 F cm^{-3} (see Fig. S10) suggesting that 80% of the capacitance remains when the current density is increased 20 times from 7.5 to 150 mA cm^{-3}. The maximum volumetric capacitance of the G@rGO-8-based supercapacitor is comparable to or even larger than those of some pseudocapacitive metal oxide-based symmetric supercapacitors (SSC) and asymmetric supercapacitors (ASC) such as C/MnO_2 SSC (0.177 F cm^{-3}) [73], MnO_2@TiN//EACC-10 ASC (2.69 F cm^{-3}) [13], MnO_2-NW//Fe_2O_3-NT ASC (1.3 F cm^{-3}, and MnO_2/graphene//VOS@C ASC (1.2 F cm^{-3}) [74]. The excellent rate capability of the G@rGO-based supercapacitor stems from the small contact resistance between the exfoliated rGO and graphite substrate and fast charge transfer through the rGO. As shown in Fig. 5**c**, the Nyquist plot suggests the total resistance of the electrolyte, separator, and contacts is 1.35 Ω and the charge transfer resistance is 0.15 Ω. The cycling performance is investigated and shown in Fig. 5**d**. The capacitance is stable even after discharging/charging for 8000 cycles at a current density of 75 mA cm^{-3} corroborating the high volumetric capacitance, excellent rate capability, and long lifetime. In addition, the gravimetric capacitance of the G@rGO symmetrical device is 33.5 F g^{-1} at a current density of 115 mA g^{-1} based on the whole mass of the device including graphene, graphite substrate, and separator as shown

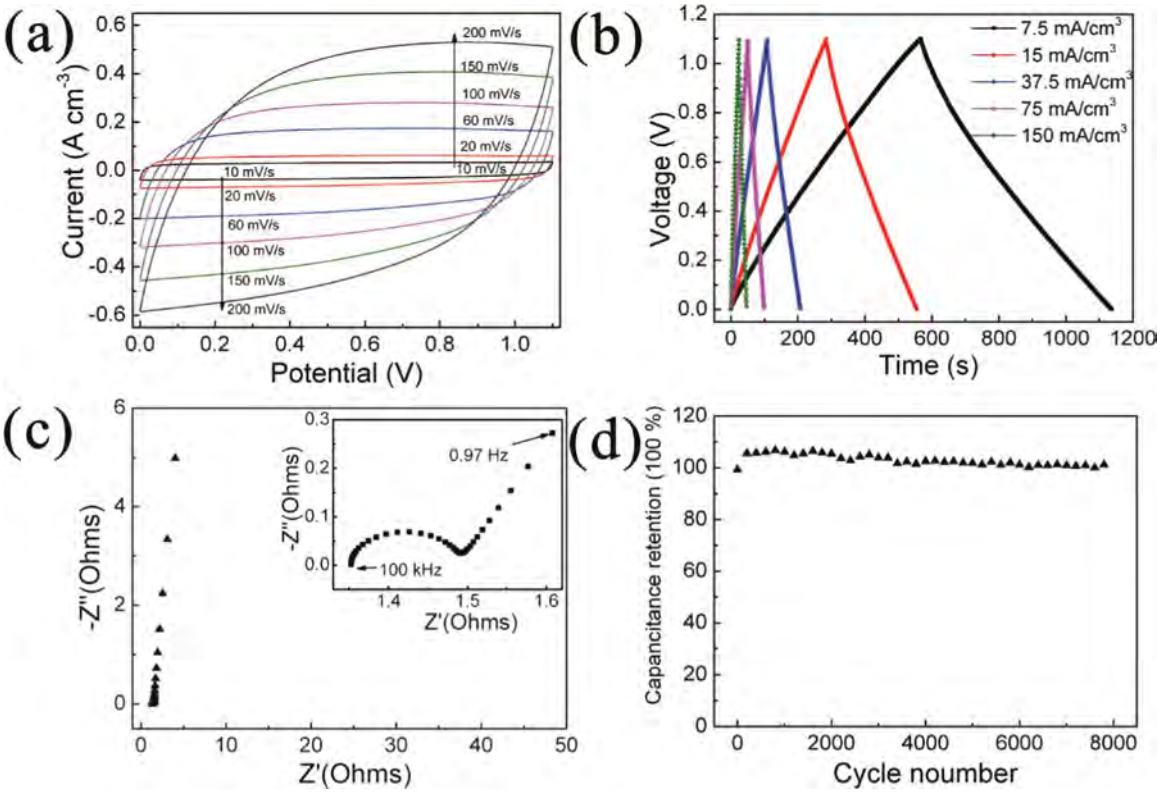

Fig. 5. Electrochemical performance of the device assembled with the G@rGO-8 electrodes: (a) CV curves at scanning rates between 10 to 200 mV s^{-1}; (b) GC curves at current densities between 7.5 and 150 mA cm^{-3}; (c) Nyquist plot; (d) Cycling performance.

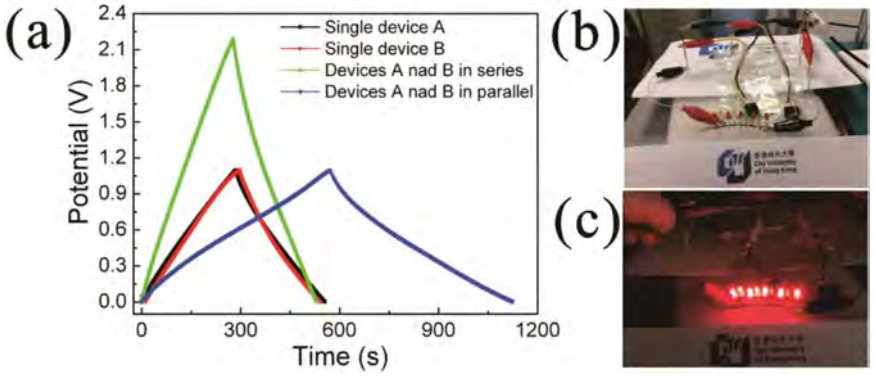

Fig. 6. (a) GC curves acquired from the two devices with different configurations: (b) Action demo showing two devices in series before (b) and after (c) lighting several LEDs in parallel.

in Fig. S11. The Ragone plots showing the energy–power characteristics of the G@rGO//G@rGO (graphite substrate included) symmetrical device reveal a maximum value of 0.66 Wh L^{-1}, which is comparable to those of other carbon and transition metal oxides based symmetrical and even some asymmetrical supercapacitors (Fig. S12) such as hydrogenated single-crystal ZnO@amorphous ZnO-doped MnO_2 core-shell nanocables on carbon cloth supercapacitors [75], H-TiO_2@MnO_2//H-TiO_2@C asymmetrical supercapacitor in an aqueous electrolyte [76], laser scribed graphene based supercapacitor in an aqueous electrolyte [2], single carbon nanotubes based supercapacitor [77], MnO_2/carbon nanoparticles based supercapacitor, and C/MnO_2 fiber-based supercapacitor [78].

To demonstrate the practical feasibility of the as-assembled supercapacitor as an energy storage component, GC tests are conducted for different configurations with two identical supercapacitors in series or parallel in the supercapacitors. The two units with similar sizes of 1.0×1.0×0.065 cm^3 (Fig. 6**b**) are designated A and B. Fig. 6**a** shows that the charging/discharging voltage window of the two supercapacitors assembled in series can reach 2.2 V for the same discharging time compared to the single supercapacitor. With regard to the assembly in parallel, the discharging time of the two supercapacitors is twice that of a single supercapacitor. The results conform to the basic rules of series and parallel assembly of capacitors. For further demonstration, two supercapacitors in series are fully charged and used to drive a series of light-emitting diodes (LEDs) assembly composed of 5 red LEDs, 2 green LEDs, and 2 yellow LEDs in parallel (Fig. 6**b**). As shown in Fig. 6**c**, all the LEDs are lit indicating promising application of the G@rGO-based supercapacitor to energy storage and electronics (see Supporting Information for the **video clip**).

Supplementary material related to this article can be found online at doi:10.1016/j.nanoen.2017.03.007.

4. Conclusion

A facile and efficient approach to produce high-density aligned graphene on graphite plate electrodes by direct anodic exfoliation of the native graphite for large-capacity supercapacitors is designed and described. The electrode consists of a ~210 μm thick graphite core and ~220 μm thick layer of the oriented reduced graphene oxide nanosheet sheath. The closely integrated core–sheath structure bodes well for supercapacitor applications because fast transportation of ions and electrons are benefited by the open structure thus resulting in small inner resistance and charge transfer resistance. The fabricated binder-free supercapacitors exhibit excellent areal capacitance (1.3 F cm^{-2}) as well as volumetric capacitance (3.9 F cm^{-3}), excellent rate performance, and long-term cycling stability. The efficient and cost-effective strategy is suitable for the development of high-performance plate electrodes having large potential in energy storage devices.

Acknowledgements

This work was jointly supported by Innovation and Technology Commission of Hong Kong, City University of Hong Kong Applied Research Grant (ARG) no. 9667122, as well as Natural Science Foundation of China (Nos.: 31500783, 51572100). KYW acknowledges the support from the Patrick S.C. Poon endowed professorship. The TEM experiments were conducted at the Hong Kong Polytechnic University Research Facility in the Materials Characterization and Device Fabrication (UMF)-center for Electron Microscopy. We acknowledge the use of the facilities and engineering support by Dr. Wei Lu and Analysis and Testing Center of HUST.

Appendix A. Supporting information

Supplementary data associated with this article can be found in the online version at doi:10.1016/j.nanoen.2017.03.007.

References

[1] J.R. Miller, R. Outlaw, B. Holloway, Science 329 (2010) 1637–1639.
[2] M.F. El-Kady, V. Strong, S. Dubin, R.B. Kaner, Science 335 (2012) 1326–1330.
[3] H. Zhu, X.L. Wang, X.X. Liu, X.R. Yang, Adv. Mater. 24 (2012) 6524–6529.
[4] F. Li, X. Jiang, J.J. Zhao, S.B. Zhang, Nano Energy 16 (2015) 488–515.
[5] C. Zhang, W. Lv, Y. Tao, Q.H. Yang, Energy Environ. Sci. 8 (2015) 1390–1403.
[6] Y. Xu, Y. Tao, X.Y. Zheng, H.Y. Ma, J.Y. Luo, F.Y. Kang, Q.H. Yang, Adv. Mater. 27 (2015) 8082–8087.
[7] P. Huang, C. Lethien, S. Pinaud, K. Brousse, R. Laloo, V. Turq, M. Respaud, A. Demortière, B. Daffos, P. Taberna, Science 351 (2016) 691–695.
[8] M. Ghidiu, M.R. Lukatskaya, M.Q. Zhao, Y. Gogotsi, M.W. Barsoum, Nature 516 (2014) 78–81.
[9] P. Simon, Y. Gogotsi, Acc. Chem. Res. 46 (2012) 1094–1103.
[10] O. Barbieri, M. Hahn, A. Herzog, R. Kötz, Carbon 43 (2005) 1303–1310.
[11] B.E. Conway, Electrochemical Supercapacitors: Scientific Fundamentals and Technological Applications, Springer Science & Business Media, 2013.
[12] G.M. Wang, H.Y. Wang, X.H. Lu, Y.C. Ling, M.H. Yu, T. Zhai, Y.X. Tong, Y. Li, Adv. Mater. 26 (2014) 2676–2682.
[13] W. Wang, W.Y. Liu, Y.X. Zeng, Y. Han, M.H. Yu, X.H. Lu, Y.X. Tong, Adv. Mater. 27 (2015) 3572–3578.
[14] J.X. Wang, S.S. Feng, Y.F. Song, W. Li, W.J. Gao, A.A. Elzatahry, D. Aldhayan, Y.Y. Xia, D.Y. Zhao, Catal. Today 243 (2015) 199–208.
[15] N.P. Wickramaratne, J.T. Xu, M. Wang, L. Zhu, L.M. Dai, M. Jaroniec, Chem. Mater. 26 (2014) 2820–2828.
[16] M. Zeiger, N. Jäckel, V.N. Mochalin, V. Presser, J. Mater. Chem. A 4 (2016) 3172–3196.
[17] Z. Li, J. Liu, K. Jiang, T. Thundat, Nano Energy 25 (2016) 161–169.
[18] R.H. Baughman, A.A. Zakhidov, W.A. de Heer, Science 297 (2002) 787–792.
[19] P. Simon, Y. Gogotsi, Nat. Mater. 7 (2008) 845–854.
[20] A. Fuertes, G. Lota, T. Centeno, E. Frackowiak, Electrochim. Acta 50 (2005) 2799–2805.
[21] P. Shang, J.N. Zhang, W.Y. Tang, Q. Xu, S.J. Guo, Adv. Funct. Mater. 26 (2016) 7766–7774.
[22] D. Liu, G. Cheng, H. Zhao, C. Zeng, D. Qu, L. Xiao, H.L. Tang, Z. Deng, Y. Li, B.L. Su, Nano Energy 22 (2016) 255–268.
[23] X.F. Wang, X.H. Lu, B. Liu, D. Chen, Y.X. Tong, G.Z. Shen, Adv. Mater. 26 (2014) 4763–4782.
[24] Y.W. Zhu, S. Murali, M.D. Stoller, K. Ganesh, W.W. Cai, P.J. Ferreira, A. Pirkle, R.M. Wallace, K.A. Cychosz, M. Thommes, Science 332 (2011) 1537–1541.
[25] R. Raccichini, A. Varzi, S. Passerini, B. Scrosati, Nat. Mater. 14 (2015) 271–279.

[26] X.W. Yang, C. Cheng, Y.F. Wang, L. Qiu, D. Li, Science 341 (2013) 534–537.
[27] Y. Tao, X.Y. Xie, W. Lv, D.M. Tang, D.B. Kong, Z.H. Huang, H. Nishihara, T. Ishii, B.H. Li, D. Golberg, F.Y. Kang, T. Kyotani, Q.H. Yang, Sci. Rep. 3 (2013) 2975.
[28] H. Li, Y. Tao, X.Y. Zheng, Z.J. Li, D.H. Liu, Z. Xu, C. Luo, J.Y. Luo, F.Y. Kang, Q.H. Yang, Nanoscale 7 (2015) 18459–18463.
[29] F. Béguin, V. Presser, A. Balducci, E. Frackowiak, Adv. Mater. 26 (2014) 2219–2251.
[30] J. Yan, Q. Wang, T. Wei, Z.J. Fan, Adv. Energy Mater. 4 (2014) 1300816.
[31] D. Li, R.B. Kaner, Nat. Nanotechnol. 3 (2008) 101.
[32] C.G. Liu, Z.N. Yu, D. Neff, A. Zhamu, B.Z. Jang, Nano Lett. 10 (2010) 4863–4868.
[33] X.W. Yang, J.W. Zhu, L. Qiu, D. Li, Adv. Mater. 23 (2011) 2833–2838.
[34] H. Li, Y. Tao, X.Y. Zheng, J.Y. Luo, F.Y. Kang, H.M. Cheng, Q.H. Yang, Energy Environ. Sci. 9 (2016) 3135–3142.
[35] J.J. Yoo, K. Balakrishnan, J. Huang, V. Meunier, B.G. Sumpter, A. Srivastava, M. Conway, A.L. Mohana Reddy, J. Yu, R. Vajtai, Nano Lett. 11 (2011) 1423–1427.
[36] Z. Bo, Z.H. Wen, H. Kim, G.H. Lu, K.H. Yu, J.H. Chen, Carbon 50 (2012) 4379–4387.
[37] S. Talapatra, S. Kar, S. Pal, R. Vajtai, L. Ci, P. Victor, M. Shaijumon, S. Kaur, O. Nalamasu, P. Ajayan, Nat. Nanotechnol. 1 (2006) 112–116.
[38] M.M. Shaijumon, F.S. Ou, L. Ci, P. Ajayan, Chem. Commun. (2008) 2373–2375.
[39] W. Chen, C. Xia, H.N. Alshareef, Nano Energy 15 (2015) 1–8.
[40] Z. Bo, W.G. Zhu, W. Ma, Z.H. Wen, X.R. Shuai, J.H. Chen, J.H. Yan, Z.H. Wang, K.F. Cen, X.L. Feng, Adv. Mater. 25 (2013) 5799–5806.
[41] D.H. Seo, S. Yick, S. Pineda, D.W. Su, G.X. Wang, Z.J. Han, K. Ostrikov, ACS Sustain. Chem. Eng. 3 (2015) 544–551.
[42] M.Z. Cai, R.A. Outlaw, R.A. Quinlan, D. Premathilake, S.M. Butler, J.R. Miller, ACS Nano 8 (2014) 5873–5882.
[43] D.H. Seo, Z.J. Han, S. Kumar, K.K. Ostrikov, Adv. Energy Mater. 3 (2013) 1316–1323.
[44] D.H. Seo, S. Yick, D.W. Su, G.X. Wang, Z.J. Han, K.K. Ostrikov, Carbon 91 (2015) 386–394.
[45] Z. Bo, S. Mao, Z.J. Han, K.F. Cen, J.H. Chen, K.K. Ostrikov, Chem. Soc. Rev. 44 (2015) 2108–2121.
[46] K.S. Novoselov, A.K. Geim, S.V. Morozov, D. Jiang, Y. Zhang, S.V. Dubonos, I.V. Grigorieva, A.A. Firsov, Science 306 (2004) 666–669.
[47] P.W. Sutter, J.I. Flege, E.A. Sutter, Nat. Mater. 7 (2008) 406–411.
[48] Y. Zhang, L.Y. Zhang, C.W. Zhou, Acc. Chem. Res. 46 (2013) 2329–2339.
[49] Y. Hernandez, V. Nicolosi, M. Lotya, F.M. Blighe, Z.Y. Sun, S. De, I. McGovern, B. Holland, M. Byrne, Y.K. Gun'Ko, J. Boland, P. Niraj, G. Duesberg, S. Krishnamurti, R. Goodhue, J. Hutchison, V. Scardaci, A.C. Ferrari, J.N. Coleman, Nat. Nanotechnol 3 (2008), 2008, pp. 563–568.
[50] J.Z. Wang, K.K. Manga, Q.L. Bao, K.P. Loh, J. Am. Chem. Soc. 133 (2011) 8888–8891.
[51] K. Parvez, Z.S. Wu, R.J. Li, X.J. Liu, R. Graf, X.L. Feng, K. Müllen, J. Am. Chem. Soc. 136 (2014) 6083–6091.
[52] W. Wei, G. Wang, S. Yang, X.L. Feng, K. Müllen, J. Am. Chem. Soc. 137 (2015) 5576–5581.
[53] S. Yang, S. Brüller, Z.S. Wu, Z.Y. Liu, K. Parvez, R.H. Dong, F. Richard, P. Samorì, X.L. Feng, K. Müllen, J. Am. Chem. Soc. 137 (2015) 13927–13932.
[54] V.V. Singh, G. Gupta, A. Batra, A.K. Nigam, M. Boopathi, P.K. Gutch, B.K. Tripathi, A. Srivastava, M. Samuel, G.S. Agarwal, Adv. Funct. Mater. 22 (2012) 2352–2362.
[55] J.L. Liu, C.K. Poh, D. Zhan, L.F. Lai, S.H. Lim, L. Wang, X.X. Liu, N.G. Sahoo, C.M. Li, Z.X. Shen, J.Y. Lin, Nano Energy 2 (2013) 377–386.
[56] C.Y. Su, A.Y. Lu, Y. Xu, F.R. Chen, A.N. Khlobystov, L.J. Li, ACS Nano 5 (2011) 2332–2339.
[57] J.H. Tang, S.S. Chen, Y. Yuan, X.X. Cai, S.J. Zhou, Biosens. Bioelectron. 71 (2015) 387–395.
[58] S. Yang, M.R. Lohe, K. Müllen, X.L. Feng, Adv. Mater. 28 (2016) 6213–6221.
[59] J.H. Lee, D.W. Shin, V.G. Makotchenko, A.S. Nazarov, V.E. Fedorov, Y.H. Kim, J.Y. Choi, J.M. Kim, J.B. Yoo, Adv. Mater. 21 (2009) 4383–4387.
[60] T.H. Kim, E.K. Jeon, Y. Ko, B.Y. Jang, B.S. Kim, H.-K. Song, J. Mater. Chem. A 2 (2014) 7600–7605.
[61] D. Li, M.B. Mueller, S. Gilje, R.B. Kaner, G.G. Wallace, Nat. Nanotechnol. 3 (2008) 101–105.
[62] I.K. Moon, J. Lee, R.S. Ruoff, H. Lee, Nat. Commun. 1 (2010) 73.
[63] J. Chastain, R.C. King, J. Moulder, Handbook of X-ray Photoelectron Spectroscopy: A Reference Book of Standard Spectra for Identification and Interpretation of XPS Data, Physical Electronics Eden Prairie, 1995.
[64] A. Ferrari, J. Robertson, Phys. Rev. B 64 (2001) 075414.
[65] K.N. Kudin, B. Ozbas, H.C. Schniepp, R.K. Prud'Homme, I.A. Aksay, R. Car, Nano Lett. 8 (2008) 36–41.
[66] A. Ambrosi, M. Pumera, Chem. Eur. J. 22 (2016) 153–159.
[67] D.L. Chao, X.H. Xia, C.R. Zhu, J. Wang, J.L. Liu, J. Lin, Z.X. Shen, H.J. Fan, Nanoscale 6 (2014) 5691–5697.
[68] L.F. Shen, Q. Che, H.S. Li, X.F. Zhang, Adv. Funct. Mater. 24 (2014) 2630–2637.
[69] X. Xiao, T.P. Ding, L.Y. Yuan, Y.Q. Shen, Q.Z. Zhong, X.H. Zhang, Y.Z. Cao, B. Hu, T. Zhai, L. Gong, J. Chen, Y.X. Tong, J. Zhou, Z.L. Wang, Adv. Energy Mater. 2 (2012) 1328–1332.
[70] X. Peng, K.F. Huo, J.J. Fu, X.M. Zhang, B. Gao, P.K. Chu, Chem. Commun. 49 (2013) 10172–10174.
[71] X. Peng, K.F. Huo, J.J. Fu, B. Gao, L. Wang, L.S. Hu, X.M. Zhang, P.K. Chu, ChemElectroChem 2 (2015) 512–517.
[72] M. Hughes, M.S. Shaffer, A.C. Renouf, C. Singh, G.Z. Chen, D.J. Fray, A.H. Windle, Adv. Mater. 14 (2002) 382–385.
[73] Q. Li, X.F. Lu, H. Xu, Y.X. Tong, G.R. Li, ACS Appl. Mater. Interfaces 6 (2014) 2726–2733.
[74] T. Zhai, X.H. Lu, Y.C. Ling, M.H. Yu, G.M. Wang, T.Y. Liu, C.L. Liang, Y.X. Tong, Y. Li, Adv. Mater. 26 (2014) 5869–5875.
[75] P.H. Yang, X. Xiao, Y.Z. Li, Y. Ding, P.F. Qiang, X.H. Tan, W.J. Mai, Z.Y. Lin, W.Z. Wu, T.Q. Li, H.Y. Jin, P.Y. Liu, J. Zhou, C.P. Wong, Z.L. Wang, ACS Nano 7 (2013) 2617–2626.
[76] X.H. Lu, M.H. Yu, G.M. Wang, T. Zhai, S.L. Xie, Y.C. Ling, Y.X. Tong, Y. Li, Adv. Mater. 25 (2013) 267–272.
[77] M. Kaempgen, C.K. Chan, J. Ma, Y. Cui, G. Gruner, Nano Lett. 9 (2009) 1872–1876.
[78] X. Xiao, T.Q. Li, P.H. Yang, Y. Gao, H.Y. Jin, W.J. Ni, W.H. Zhan, X.H. Zhang, Y.Z. Cao, J.W. Zhong, L. Gong, W.C. Yen, W.J. Mai, J. Chen, K.F. Huo, Y.L. Chueh, Z.L. Wang, J. Zhou, ACS Nano 6 (2012) 9200–9206.

Liangsheng HU received his BS and MS from Wuhan University of Science and Technology in 2007 and 2011, respectively. He is a PhD candidate in chemistry of The Hong Kong Polytechnic University. His research focuses on the synthesis and application of functional nanomaterials for (electro)photochemical energy conversion and storage.

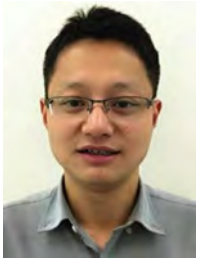

Xiang Peng is a PhD candidate under the supervision of Prof. Paul K. Chu in the Department of Physics and Materials Science, City University of Hong Kong. His research focuses on synthesis of functional nanomaterials and fabrication of electrochemical energy storage devices for supercapacitors, Li-ion batteries, and electrocatalytic applications.

Yong Li received his BS and MS from Wuhan University of Science and Technology in 2011 and 2014, respectively. He worked at the Shenzhen Institutes of Advanced Technology, Chinese Academy of Sciences from 2014 to 2016. Currently, he works at The Hong Kong Polytechnic University as a research assistant. His research focuses on nanostructured materials for electrocatalysis and electrochemical sensors.

Lei Wang earned his B.S. in physics from Huazhong University of Science and Technology (HUST) in 2012. He is pursuing his PhD in the Wuhan National Laboratory for Optoelectronics (WNLO) at Huazhong University of Science and Technology (HUST), under the supervision of Prof. Kaifu Huo. His present research interest is synthesis and characterization of nanostructured electrode architectures and materials for electrochemical energy conversion and storage.

Kaifu Huo received his BS in applied chemistry from China University of Petroleum in 1997 and a PhD in physical chemistry from Nanjing University (China) in 2004. He is currently Professor in the National Laboratory for Optoelectronics at Huazhong University of Science and Technology. He is an associate editor of Nanoscience and Nanotechnology Letters (NNL). He has authored/co-authored more than 100 papers in international refereed journals with over 3000 citations (H-index=30). His main research activities encompass bioactive nanomaterials and nanostructured electrode materials for electrochemical biosensors and energy storage devices.

Lawrence Yoon Suk Lee received his PhD from McGill University, Canada in 2006. He is now a research assistant professor at the Hong Kong Polytechnic University. His research interests include development of novel semiconductor nanomaterials for photocatalytic water splitting and CO_2 reduction as well as electrode materials for lithium ion batteries.

Kwok-yin Wong is Patrick S.C. Poon Endowed Professor in Applied Chemistry, Chair Professor of Chemical Technology, and director of the Partner State Key Laboratory of Chirosciences at The Hong Kong Polytechnic University. He obtained his BSc(Hons) and PhD in chemistry from The University of Hong Kong in 1981 and 1986, respectively. He was a postdoctoral research fellow at California Institute of Technology (USA) from 1986 to 1987. His main research areas include electrochemistry, green chemistry, biosensors and antibiotics development. He has published over 180 SCI journal articles and is the holder of 6 international patents.

Paul K. Chu received his BS in mathematics from The Ohio State University and MS/PhD in chemistry from Cornell University. He is Chair Professor of Materials Engineering in the Department of Physics and Materials Science at City University of Hong Kong. His research interests are quite diverse encompassing plasma surface engineering, materials science and engineering, surface science, and functional materials. He is Fellow of the American Physical Society (APS), American Vacuum Society (AVS), Institute of Electrical and Electronics Engineers (IEEE), Materials Research Society (MRS), and Hong Kong Institution of Engineers (HKIE). He is also Fellow of the Hong Kong Academy of Engineering Sciences (HKAES) and on the member committee of HKAES. He is a highly cited researcher in materials science according to Thomson Reuters.

Supporting Information

Direct Anodic Exfoliation of Graphite onto High-density Aligned Graphene for Large Capacity Supercapacitors

Liangsheng Hu[a,1], Xiang Peng[b,1], Yong Li[a], Lei Wang[c], Kaifu Huo[c,*], Lawrence Yoon Suk Lee[a], Kwok-Yin Wong[a,*], Paul K Chu[b,*]

[a] Department of Applied Biology and Chemical Technology and the State Key Laboratory of Chirosciences, The Hong Kong Polytechnic University, Hung Hom, Hong Kong, P.R. China.

[b] *Department of Physics and Materials Science, City University of Hong Kong, Tat Chee Avenue, Kowloon, Hong Kong, China.*

[c] *Wuhan National Laboratory for Optoelectronics (WNLO) and School of Optical and Electronic Information, Huazhong University of Science and Technology, Wuhan 430074, China.*

*Corresponding authors.
E-mail addresses: kwok-yin.wong@polyu.edu.hk (K.-Y.Wong), paul.chu@cityu.edu.hk (P.K. Chu), kfhuo@hust.edu.cn (K.F. Huo)

[1] These authors contributed equally to this work

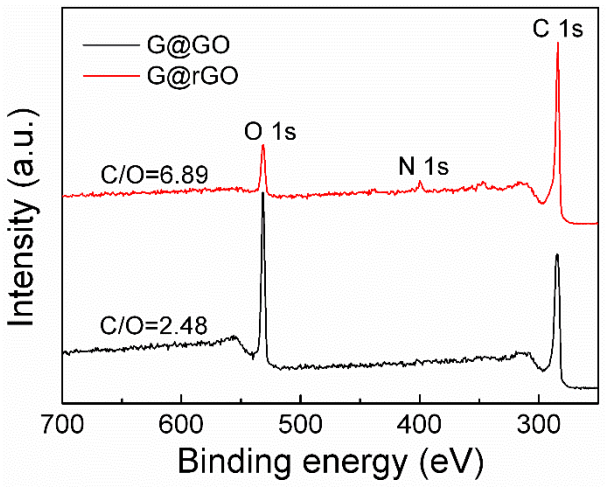

Fig. S1. XPS survey scans of G@GO and G@rGO.

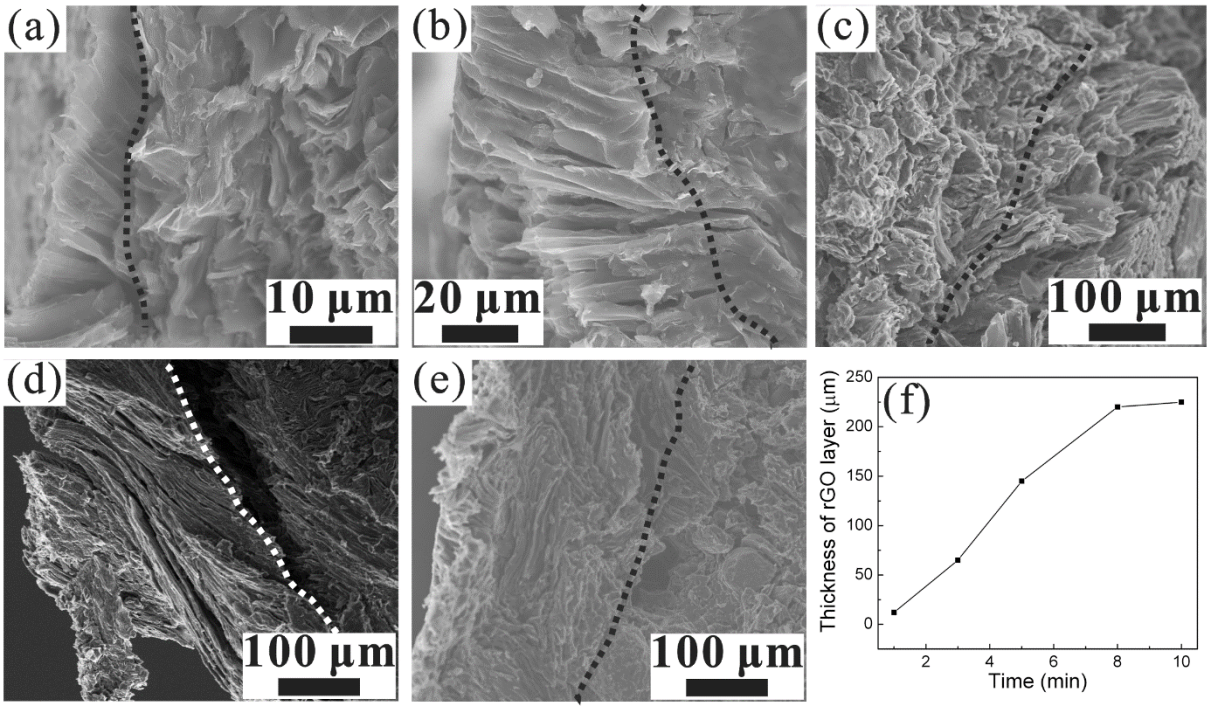

Fig. S2. Longitudinal views of G@rGO for different oxidation time: (a) 1 min, (b) 3 min, (c) 5 min, (d) 8 min, and (e) 10 min; (f) Thickness of the rGO layers for different oxidation time.

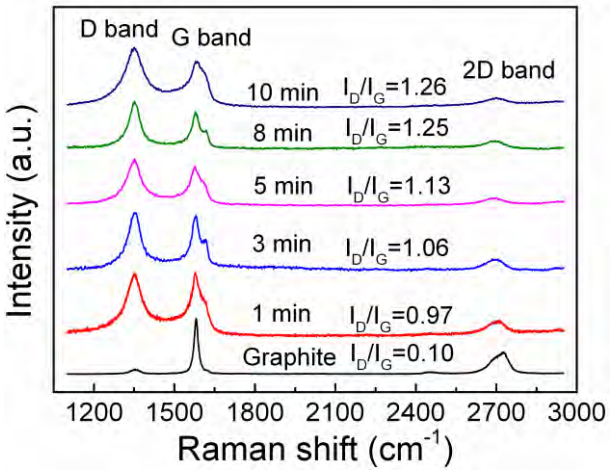

Fig. S3. Raman spectra of G@rGO for different exfoliation time.

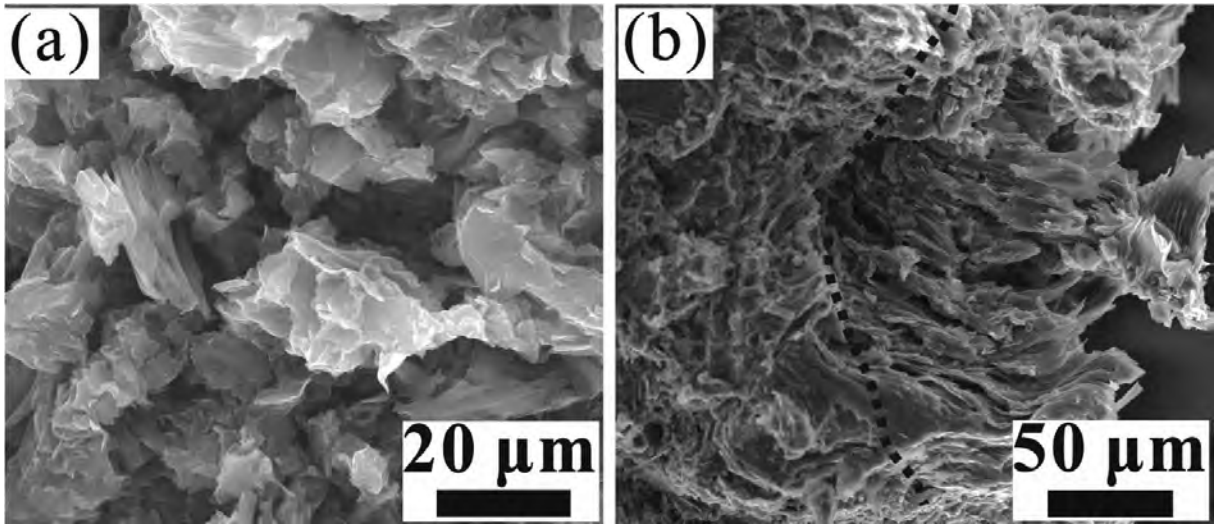

Fig. S4. FE-SEM images: (a) Top and (b) Longitudinal views of G@rGO treated at room temperature.

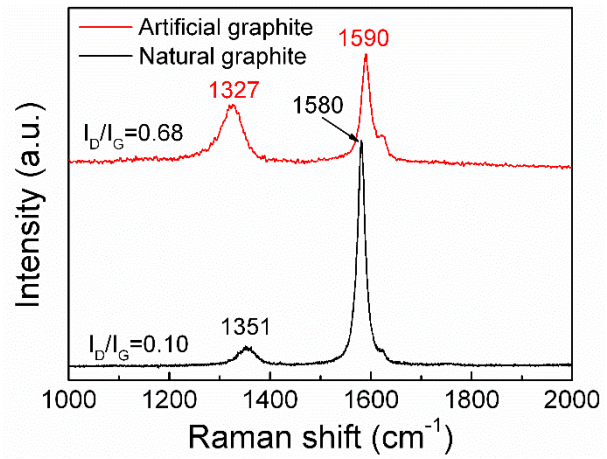

Fig. S5. Raman scattering spectra of different kinds of pristine graphite.

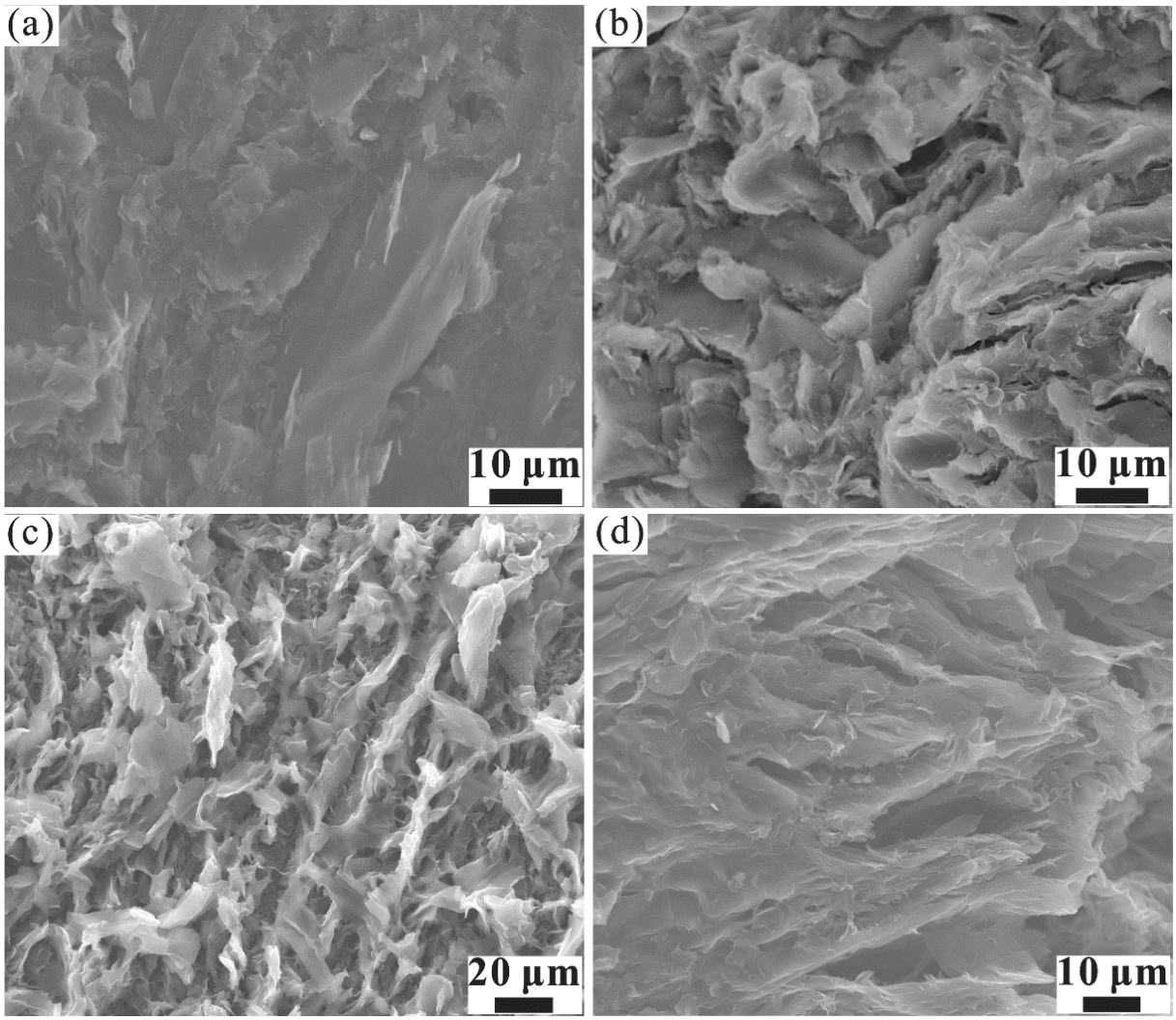

Fig. S6. FE-SEM images: (a) Top and (b) Cross-sectional views of artificial graphite; (c) Top and (d) Longitudinal views of G@GO fabricated from artificial graphite.

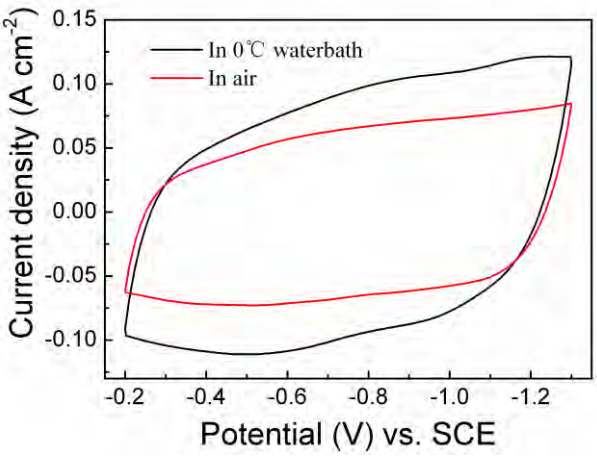

Fig. S7. Comparison of CV curves of G@rGO electrodes fabricated in a 0 ºC water bath at room temperature (in air).

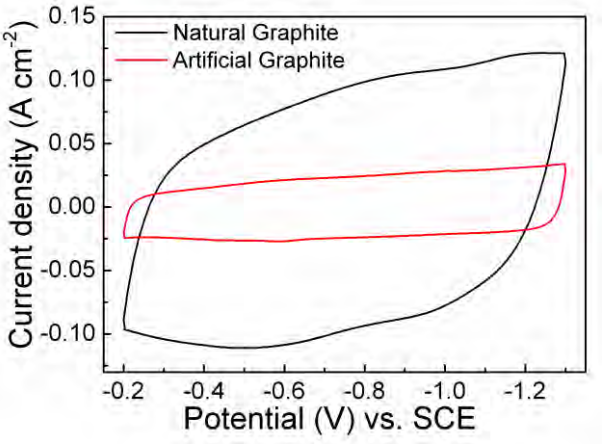

Fig. S8. Comparison of CV curves of G@rGO electrodes oxidized from artificial graphite and natural graphite.

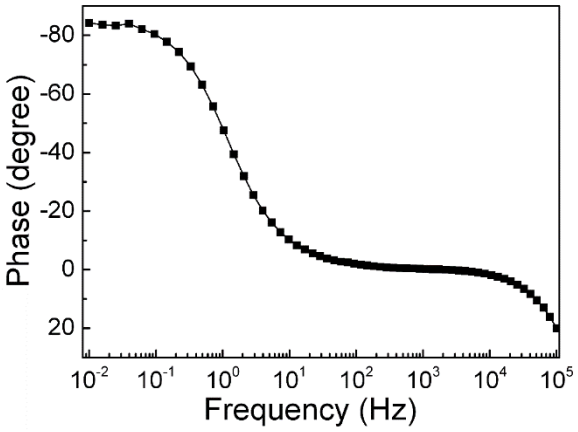

Fig. S9. Relationship between the phase angle and frequency of G@rGO-8.

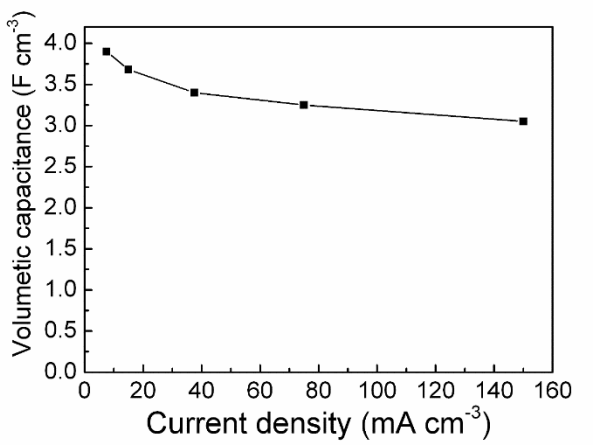

Fig. S10. Volumetric capacitance as a function of current density of the G@rGO-8 based supercapacitor.

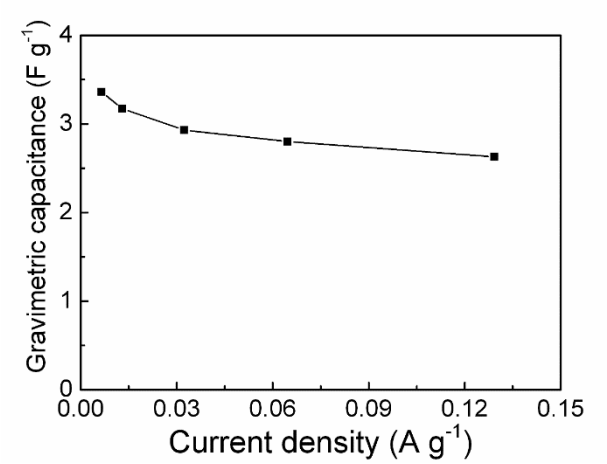

Fig. S11. Gravimetric capacitance as a function of current density of the G@rGO-8 based supercapacitor (including graphite substrate).

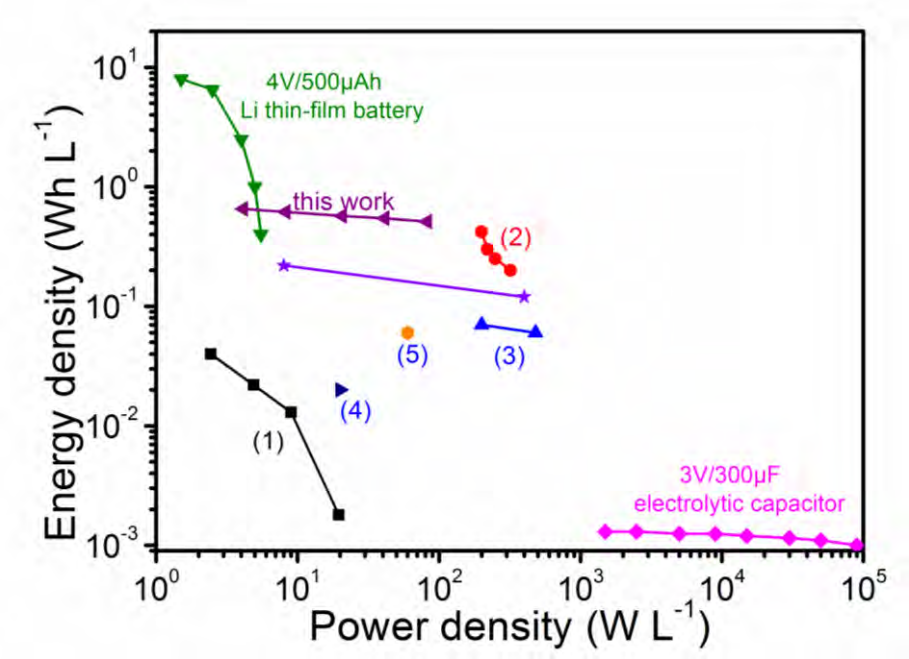

Fig. S12. Ragone plot of the G@rGO based supercapacitor compared with reported values: (1) Hydrogenated single-crystal ZnO@amorphous ZnO-doped MnO_2 core-shell nanocables on a carbon cloth supercapacitor [1], (2) H-TiO_2@MnO_2//H-TiO_2@C asymmetrical supercapacitor in an aqueous electrolyte [2], (3) Laser scribed graphene based supercapacitor in an aqueous electrolyte [3], (4) Single carbon nanotubes based supercapacitor [4], (5) MnO_2/carbon nanoparticles based supercapacitor, and (6) C/MnO_2 fiber-based supercapacitor [5].

Table S1 Comparison of the volumetric capacitance of G@rGO based supercapacitor in this work with other reported systems.

Devices	Electrolyte	maximum capacitance	Ref.
G@rGO/G@rGO	6M KOH	3.9 F cm^{-3}	This work
C/MnO_2/C/MnO_2	1M Na_2SO_4	0.177 F cm^{-3}	[6]
H-TiO_2@MnO_2//H-TiO_2@C	5M LiCl	0.9 F cm^{-3}	[2]
Carbon onions Microsupercapacitor	1M Et_4NBF_4/anhydrous propylene carbonate	1.3 F cm^{-3}	[7]
Graphene Microsupercapacitors	PVA-H_2SO_4	3.05 F cm^{-3}	[8]
Graphene based supercapacitor	1M H_3PO_4	0.5 F cm^{-3}	[3]

References

[1] P.H. Yang, X. Xiao, Y.Z. Li, Y. Ding, P.F. Qiang, X.H. Tan, W.J. Mai, Z.Y. Lin, W.Z. Wu, T.Q. Li, H.Y. Jin, P.Y. Liu, J. Zhou, C.P. Wong, Z.L. Wang, ACS Nano 7 (2013) 2617-2626.

[2] X.H. Lu, M.H. Yu, G.M. Wang, T. Zhai, S.L. Xie, Y.C. Ling, Y.X. Tong, Y. Li, Adv. Mater. 25 (2013) 267-272.

[3] M.F. El-Kady, V. Strong, S. Dubin, R.B. Kaner, Science 335 (2012) 1326-1330.

[4] M. Kaempgen, C.K. Chan, J. Ma, Y. Cui, G. Gruner, Nano Lett. 9 (2009) 1872-1876.

[5] X. Xiao, T.Q. Li, P.H. Yang, Y. Gao, H.Y. Jin, W.J. Ni, W.H. Zhan, X.H. Zhang, Y.Z. Cao, J.W. Zhong, L. Gong, W.C. Yen, W.J. Mai, J. Chen, K.F. Huo, Y.L. Chueh, Z.L. Wang, J. Zhou, ACS Nano 6 (2012) 9200-9206.

[6] Q. Li, X.F. Lu, H. Xu, Y.X. Tong, G.R. Li, ACS Appl. Mater. Interfaces 6 (2014) 2726-2733.

[7] D. Pech, M. Brunet, H. Durou, P.H. Huang, V. Mochalin, Y. Gogotsi, P.L. Taberna, P. Simon, Nat. Nanotechnol. 5 (2010) 651-654.

[8] M.F. El-Kady, R.B. Kaner, Nat. Commun. 4 (2013) 1475